BOUNDARY CONDITIONS IN LINEAR 3D-AEROACOUSTIC NUMERICAL SIMULATION

M. Pospiech, P. Rentrop
Technische Universität München, Centre for Mathematical Sciences

Corresponding author: M.Pospiech, email: pospiech@ma.tum.de
Technische Universität München (M2), Boltzmannstraße 3, 85748 Garching

Abstract. The focus of this contribution lies in the modelling, analysis and simulation of realistic boundary conditions. We are especially concentrating on wave number dependent boundaries including reflection, transmission and absorption of acoustic waves. The realistic treatment of boundary conditions within accurate aeroacoustic simulations is of interest for [1], [5] et alii.
Our numerical research deals with the Spectral Method for a 3D-benchmark problem. To introduce the spectral approach [3] we study the homogeneous Helmholtz equation in a 3D cuboid benchmark geometry. After developing the theory, numerical results of the calculated Eigenmodes and related Eigenfrequencies for different boundary conditions will be discussed.

1 Introduction

Aeroacoustic starts from the Euler equations describing the conservation of pressure p, density ρ and velocity u in a fluid

$$\begin{pmatrix} \rho \\ \rho u \\ \rho E \end{pmatrix}_t + \begin{pmatrix} \rho u \\ \rho u^2 \\ u(\rho E + p) \end{pmatrix}_x = 0 \ . \tag{1}$$

The ideal gas equation

$$p \ = \ \rho R T \tag{2}$$

closes the system. In (1) and (2) E denotes the energy, R the Boltzmann constant and T the temperature. In (1) we study the 1D case with a homogeneous right side which can be easily expanded to the 3D Euler equations.
Because we are only interested in the far field, a perturbation ansatz in all three variables is performed

$$\begin{array}{rcl} \rho(x,t) & = & \rho_0 + \rho'(x,t) \\ p(x,t) & = & p_0 + p'(x,t) \\ u(x,t) & = & u_0 + u'(x,t) \qquad (u_0 = 0) \ . \end{array} \tag{3}$$

With the linearized pressure-density-relation $p' = \rho' c^2$, where c stands for the sound velocity, we arrive at the linear Euler equations in one dimension

$$\begin{array}{rcl} \rho'_t + \rho_0 u'_x & = & 0 \\ u'_t + \frac{c^2}{\rho_0} \rho'_x & = & 0 \ . \end{array} \tag{4}$$

After a reformulation of the equations in (4) we end up with the hyperbolic Wave equation for each perturbed variable u', ρ' and p'. This derivation can be easily expanded to three dimensions in space x, y and z and would end up in the three dimensional Wave equation for each perturbed variable. That leads to our first central formula, the 3D Wave equation for the pressure

$$p'_{tt} \ = \ c^2 \Delta p' \ . \tag{5}$$

The Wave equation (5) stands for the dispersion free and dissipation free wavelike transport of information with finite velocity c.
Considering the time harmonical problem we get to the steady-state solution of the Wave equation represented by the 3D Helmholtz equation in the frequency domain

$$\Delta p' + k^2 p' = 0, \qquad c^2 = \frac{\omega^2}{k^2}, \quad k^2 = k_x^2 + k_y^2 + k_z^2 \ . \tag{6}$$

One possibility to develop the Helmholtz equation (6) from the Wave equation (5) is to apply the Fourier transformation. In (6) ω stands for the circular frequency and k for the wavenumber. For both the Wave equation (5) as well as the Helmholtz equation (6) we analyse the solution in dependency of general homogeneous boundary conditions

$$\left[\alpha \frac{\partial p'}{\partial n} + \beta p'\right]_{\partial\Omega} = 0, \qquad \alpha, \beta \in \mathbb{C} \ . \tag{7}$$

In formula (7) different combinations are possible. For $\alpha = 0$ and $\beta \neq 0$ we end up in the Dirichlet, for $\alpha \neq 0$ and $\beta = 0$ in the Neumann and for $\alpha \neq 0$ and $\beta \neq 0$ in the Robin boundary condition. The ratio $\frac{\alpha}{\beta}$ stands for the wall impedance. In the following sections p is used for p' and an apostrophe stands for the first derivative in x.

The paper is organised as follows: In chapter 2 the theory of the Spectral Method is presented with the help of the one dimensional Helmholtz equation described by the pressure p. First we analyse the method for equispaced grids and then for clustered grids. After that we discuss the convergence relationships, the application of higher dimensional problems and the inclusion of arbitrary homogeneous boundary conditions. In chapter 3 we verify the theoretic characteristics of the method for selected examples in the time and frequency domain for the related Wave as well as the Helmholtz equation. At the end in chapter 4 follow the conclusions and objectives.

2 Theory of the Spectral Method

For simplicity we derive the method by using the one dimensional case of the Helmholtz equation described by the pressure p in the frequency domain, see (6). In the Spectral Method all spatial differentiation operators are described as global differentiation operators. Consequently the one dimensional continuous Helmholtz equation in p after discretization leads to the discrete eigenvalue problem described in a matrix vector equation

$$L_N p + k^2 I p = 0, \qquad N \in \mathbb{N} \ . \tag{8}$$

In (8) L_N stands for the discrete Laplacian and I denotes the identity matrix. The method makes use of a global differentiation technique based on trigonometric or Chebyshev interpolation and gains spectral accuracy for analytic solutions, which will be presented in the next three subsections. The last subsection deals with higher dimensional problems and how to include boundary conditions.

Spectral Collocation in Equispaced Grids in 1D

As a first step we define the one dimensional interpolant u of the sufficient smooth solution p by

$$u(x) = \sum_{j=1}^{N} p_j S_h(x - x_j), \qquad p_j = p(x_j) = u(x_j), \quad x \in \Omega = [-\pi, \pi] \ . \tag{9}$$

The interpolant, described by means of equidistant supporting points x_j

$$x_j = jh \ , \qquad j = 0, \ldots, N, \quad h = \frac{2\pi}{N},$$

is symmetric around zero and normalized. Therefore S_h is defined as

$$S_h(x) = \frac{h \sin(\frac{x\pi}{h})}{2\pi \tan(\frac{x}{2})} \ .$$

and behaves similar to the Sinus Cardinalis function

$$sinc(x) = \frac{sin(x)}{x} \ .$$

This realizes a symmetric Lagrange representation with trigonometric functions of the interpolant for the periodic function $p(x)$ in (9).
After differentiating equation (9) we arrive at

$$u'(x) = \sum_{j=0}^{N} p_j S_h'(x - x_j)$$

and consequently the first differentiation matrix D_N consists of the following elements

$$(D_N)_{jk} = S_h'(x_j - x_k) = \frac{(-1)^{(j-k)}}{2} \cot(\frac{(j-k)h}{2}), \quad j, k = 0, \ldots, N \ . \tag{10}$$

The differentiation can now be written in matrix vector notation as

$$\begin{pmatrix} u'(x_1) \\ u'(x_2) \\ \vdots \\ u'(x_N) \end{pmatrix} = D_N \begin{pmatrix} u(x_1) \\ u(x_2) \\ \vdots \\ u(x_N) \end{pmatrix} .$$

Equation (10) shows, that D_N is a circulant skew-symmetric Toeplitz matrix and all its diagonal elements are zero, because of

$$\lim_{x\to 0} S_h'(x) \quad = \quad 0 \ .$$

For the second differentiation matrix D_N^2 we end up in

$$(D_N^2)_{jk} \quad = \quad S_h''(x_j - x_k) \quad = \quad \begin{cases} -\frac{\pi^2}{3h^2} - \frac{1}{6}, & j = k \\ -\frac{(-1)^{(j-k)}}{2\sin^2(\frac{(j-k)h}{2})}, & j \neq k \end{cases}, \ j,k = 0,...,N, \tag{11}$$

which again is a circulant skew-symmetric Toeplitz matrix. In this case all diagonal elements are constant as described in (11).

Spectral Collocation in Clustered Grids in 1D

In this subsection we analyse nonperiodic functions $p(x)$. Therefore we change our trigonometric approach in equation (9) and use algebraic polynomials for the interpolation instead. This is useful, because equispaced grids may develop instabilities at the boundaries, known as the Runge phenomenon. A way out are sets of clustered points, distributed with the density

$$\text{density} \quad \sim \quad \frac{N}{\pi\sqrt{1-x^2}},$$

assuming a transformation of our problem to $\Omega = [-1,1]$. As a starting point consider, that the interpolant has the following Lagrange form

$$u_N(x) \quad = \quad \omega_{N+1}(x) \sum_{j=0}^{N} \frac{p_j}{(x-x_j)\omega_{N+1}'(x_j)} \in \Pi_N \quad , \quad \omega_N(x) = \prod_{j=0}^{N} (x - x_j) \ .$$

For every supporting point x_j there is a weight

$$\lambda_j \quad = \quad \frac{1}{\omega_{N+1}'(x_j)}$$

and with

$$1 \quad = \quad \omega_{N+1} \sum_{j=0}^{N} \frac{\lambda_j}{(x-x_j)}$$

follows the stable barycentric form

$$u_N(x) \quad = \quad \frac{\sum_{j=0}^{N} \frac{\lambda_j p_j}{(x-x_j)}}{\sum_{j=0}^{N} \frac{\lambda_j}{(x-x_j)}} \ .$$

All interpolants of this kind cluster at the boundaries and consequently the points occur with higher probability at the interval endpoints.
Finally we restrict our focus to one representative, the Chebyshev interpolant. For this purpose we take the Chebyshev-Gauss-Lobatto collocation points

$$x_j \quad = \quad \cos(\tfrac{j\pi}{N}), \qquad j = 0,...,N, \tag{12}$$

which are the extremas of the n-th order Chebyshev polynomials of the first kind

$$T_N(x) \quad = \quad \cos(N \arccos(x)) \ .$$

In this case the interpolant takes the form

$$u_N(x) \quad = \quad \omega_{N+1} \sum_{j=0}^{N} p_j g_j(x), \qquad g_j(x_k) = \delta_{jk}$$

with

$$g_j(x) = \frac{(-1)^{j+1}(1-x^2)T'_N(x)}{c_j N^2 (x-x_j)}, \qquad c_j = \begin{cases} 2 & , j=0 \vee j=N \\ 1 & , j=1,...,N-1 \end{cases} . \tag{13}$$

After taking the analytical derivative of (13) we get the elements of the Chebyshev derivative matrix D_N at the collocation points

$$\begin{aligned} (D_N)_{00} &= \tfrac{2N^2+1}{6}, \qquad (D_N)_{NN} = -(D_N)_{00}, \\ (D_N)_{ii} &= \tfrac{-x_i}{2(1-x_i^2)}, \qquad i=1,...,N-1, \\ (D_N)_{ij} &= \tfrac{c_i\,(-1)^{i+j}}{c_j(x_i-x_j)}, \quad i\neq j,\ i,j=0,1,...,N\ . \end{aligned} \tag{14}$$

The second Chebyshev derivative matrix D_N^2 can be determined with the help of (14), $D_N^2 = (D_N)^2$. Analogously any further higher Chebyshev derivative matrix can be computed in the same way $D_N^\nu = (D_N)^\nu$, $\nu \in \mathbb{N}$. For further details see [7] and [4].

Convergence Analysis

Now we are able to discuss the accuracy properties of the method. For analytic functions p we will show the convergence $O(c^N)$, where c is an arbitrary constant with $0 < c < 1$, known as spectral accuracy. For smooth functions there will be the typical convergence rate $O(N^m)$, $m \in \mathbb{N}$, see [7].
These relationships can be derived by Fourier transformation for $p \in L^2$

$$\begin{aligned} p(x) \quad &\overset{\textit{fourier transformation}}{\rightarrow} \quad \hat{p}(k) = \int_{-\infty}^{+\infty} e^{-ikx}u(x)dx \\ \hat{p}(k) \quad &\overset{\textit{inverse fourier transformation}}{\rightarrow} \quad p(x) = \tfrac{1}{2\pi}\int_{-\infty}^{+\infty} e^{+ikx}\hat{u}(k)dk, \end{aligned}$$

because smooth functions have fast decaying transformations and consequently the aliasing error is small. That means the error of the interpolant $u(x)$ (see equation (9)) is in direct dependency of the decay behavior of the function $\hat{p}(k)$, which depends on the smoothness of the function $p(x)$ in the space domain.
For $p \in C^{(d-1)}$ and $p^{(d)}$ having bounded variation it follows, that $\hat{p}(k) \in O(k^{-(d+1)})$ for $k \to \infty$. This justifies the estimation of the aliasing error in the frequency domain

$$\begin{aligned} |\hat{p}(k)-\hat{u}(k)| &= \begin{cases} |\sum\limits_{j\in\mathbb{Z}\setminus h}\hat{p}(k+\frac{2\pi j}{h})| \le |c\sum\limits_{j\in\mathbb{Z}\setminus h}|k+\frac{2\pi j}{h}|^{-(d+1)}| \\ |\hat{p}(k)| \le c|k|^{-(d+1)} \end{cases} \\ &\le \begin{cases} ch^{d+1}\sum\limits_{j\neq 0}|kh+2\pi j|^{-(d+1)}|, & |k| \neq \frac{\pi}{h} \\ O(h^{d+1}), & |k| > \frac{\pi}{h} \end{cases} \\ &= 0, \quad \text{for } h\to 0 \text{ and } d \ge 1 \end{aligned}$$

and the interpolation error in the space domain

$$\begin{aligned} |p(x)-u(x)| &= |\tfrac{1}{2\pi}\int_{-\infty}^{+\infty} e^{+ikx}\hat{p}(k)dk - \tfrac{1}{2\pi}\int_{|k|\le\frac{\pi}{h}} e^{+ikx}\hat{u}(k)dk| \\ &= |\tfrac{1}{2\pi}\int_{|k|\le\frac{\pi}{h}} e^{+ikx}(\hat{p}-\hat{u})(k)dk - \tfrac{1}{2\pi}\int_{|k|>\frac{\pi}{h}} e^{+ikx}\hat{u}(k)dk| \\ &\le \tfrac{1}{2\pi}\tfrac{\pi}{h}O(h^{d+1}) + \tfrac{1}{2\pi}\int_{|k|>\frac{\pi}{h}} O(k^{-(d+1)})dk \\ &= O(h^d)+O(h^d) = O(h^d)\,. \end{aligned}$$

It is now possible to expand the interpolation error for arbitrary derivatives

$$|p^{(\nu)}(x) - u^{(\nu)}(x)| \quad = \quad O(h^{d-\nu}) \quad \text{for } h \to 0 \text{ and } d \geq \nu + 1 \tag{15}$$

if $p \in C^{(d-1)}$ and $p^{(\nu)}$ has bounded variation. For the stricter constraint $u \in C^{\infty}$ we can follow

$$|p^{(\nu)}(x) - u^{(\nu)}(x)| \quad = \quad O(h^m) \quad \forall m \in \mathbb{N} \tag{16}$$

and if u even is an analytic function, we end up in the so called spectral accuracy

$$|p^{(\nu)}(x) - u^{(\nu)}(x)| \quad = \quad O(e^{-\frac{c}{h}}) \quad c \in \mathbb{R}\,. \tag{17}$$

With (15), (16) and (17) the most important convergence theorems are summarized. For more details see [7].

Boundary Conditions and Tensor Product Grids in Higher Dimensions

The Spectral Method enables the realisation of arbitrary boundary conditions as we have seen in (7). Prescribed boundary conditions have to be included in the derivative matrix D_N^{ν}, $\nu \in \mathbb{N}$, where ν depends on the underlying problem. If we require a Neumann boundary condition at the left endpoint and a Robin boundary condition at the right endpoint of the 1D Helmholtz equation, then it has the form

$$\alpha \frac{\partial p}{\partial n}(x) = 0, \quad x = -1, \qquad \text{and} \quad \beta \frac{\partial p}{\partial n}(x) + \gamma p(x) = 0, \quad x = 1.$$

These constraints have to be directly inserted into the second Chebyshev derivative matrix of the related matrix vector equation (8) as follows

$$L_N = D_N^2 \rightarrow \quad \widetilde{L}_N = \widetilde{D}_N^2 \qquad = \begin{bmatrix} \widetilde{D}_N^2(1,:) \\ - - - - - - - - - - - - - - - \\ \\ D_N^2(2:N,:) \\ \\ - - - - - - - - - - - - - - - \\ \widetilde{D}_N^2(N+1,:) \end{bmatrix} \in \mathbb{R}^{(N+1)\times(N+1)} \tag{18}$$

$$\text{with} \qquad \widetilde{D}_N^2(1,:) \quad = \quad \beta D_N(1,:) \quad + \quad \gamma[1\ 0\ \ldots\ 0]\,,$$

$$\widetilde{D}_N^2(N+1,:) \quad = \quad \alpha D_N(N+1,:)\,.$$

For boundary problems where different conditions occur at the same boundary the procedure is not straight forward. For example, a least square approach or a polynomial including different boundary conditions are possible, but then lead to different convergence rates.

Finally let us consider higher dimensional differential equations like the 3D Helmholtz equation (6). Because of the global approach only simple geometries like cubes, spheres and cylinders are possible. To calculate in higher dimensions we make use of tensor product grids realised as Kronecker products. The ordering of the single matrices inside the Kronecker product depends on the underlying programing language. To end up in $\widetilde{L}_N$ the problem-specific conditions have to be incorporated in every single D_N^2 of the partial derivatives with the corresponding boundary conditions, compare (18). Obviously the degrees of freedom increase exponentially with growing dimension d. Consequently it is getting very expensive, because the size of the matrices. The costs are growing with N^d. For more details see the appendix in chapter 5 and [7].

3 Numerical Simulations

Example in the Time Domain

As a first example we want to show the advantages for calculations in the time domain. Therefore we take the geometry $\Omega = [-1,1]$ and the 1D Wave equation $p(x,t)_{tt} = c^2 \Delta p(x,t)$ with $c = 1$. The meshgrid is clustered, see (12), with $N = 100$ and the initial values are given by

$$p(x,0) \;=\; e^{\frac{-1}{(x-a)^2(x-b)^2}+\frac{1}{(ab)}}, \quad a=-0.5,\; b=0.5 \qquad \text{with } \; p(x,0) := 0 \;\text{ for }\; |x| \geq 0.5\,. \tag{19}$$

We enforce homogeneous Dirichlet boundary conditions in the second Chebyshev derivative matrix as explained in (18) and in the initial values. This problem gives reason to identify the simulated solution $p(x,t)$ with the sound particle velocity in acoustics instead of the pressure. For the second derivative in time we choose the second order Leapfrog method. To study the behavior in the long-term integration we choose $\Delta t = 4/N^2$ as a stable time step. Because of the symmetry and the defined sound velocity c, the propagated initial values (19) overlap after 2500 time steps in the middle of Ω alternately to the original shape and to the negative original shape. To analyse the dissipation error we calculate the energy of the solution

$$\int_{\Omega} (p(x,t)_t)^2 \;+\; (p(x,t)_x)^2 \;\, dx$$

in every time step. Altogether we simulate over 500000 time steps, that means 500 periods and 1000 reflections at the boundaries. In that long-term integration the energy (3) varies less than 3 percent. The same example in a 3D sphere with related initial conditions gives approximately equivalent results. Although the error of the second order time stepping method is dominant, there are no conspicuous spurious oscillations. Both of the above mentioned difficulties are typical in finite difference and related optimized DRP schemes [6] applied to (4) and (5). By the way for high order methods like the ADER method [5] with a low dispersion and dissipation error extensive effort is needed to insert boundary conditions.
Consequently the combination of the spectral method for the space derivative and a low order method for the time derivative is advantageous for long-term integrations and a low dissipation error.

Examples in the Frequency Domain

In the second example we want to analyse is the Helmholtz equation (8) for an arbitrary cuboid in $\mathbb{R}^3$. As a representative we define the geometry Ω and prescribe reverberative boundary conditions

$$\Omega = \quad [-1,1]^3, \qquad \frac{\partial p}{\partial n}(\vec{x}) = \quad 0, \quad \forall x \in \partial\Omega,$$

relating to a simple room with completely reflecting walls. The analytic solution for the Eigenmodes of this example is given by the infinite discrete spectrum

$$p(\vec{x}) = \sum_{i,j,k=1}^{\infty} a_{ijk} \cos(\frac{\pi i}{2}x)\cos(\frac{\pi j}{2}y)\cos(\frac{\pi k}{2}z), \quad a_{ijk} \in \mathbb{R}$$

and the related Eigenfrequencies can be described with the help of the wavenumber

$$k_{ijk} \;= \sqrt{k_x^2+k_y^2+k_z^2} = \sqrt{(\frac{\pi i}{2})^2+(\frac{\pi j}{2})^2+(\frac{\pi k}{2})^2}, \quad i,j,k = 1,\ldots,\infty, \quad \omega_{ijk} = k_{ijk}c \;.$$

We use an in Matlab implemented Spectral Method code to solve the problem. The spectral convergence rates for the first 4 different Eigenfrequencies can be seen in figure 1.

In detail we see the convergence rates of the first four different Eigenfrequencies, ω_{111}, ω_{211}, ω_{221} and ω_{311}, which are directly related to the first four different wave numbers as shown in equation (6). The figure also represents the exponential decrease of the relative error in dependency of the degrees of freedom growing with $(N+1)^3$.

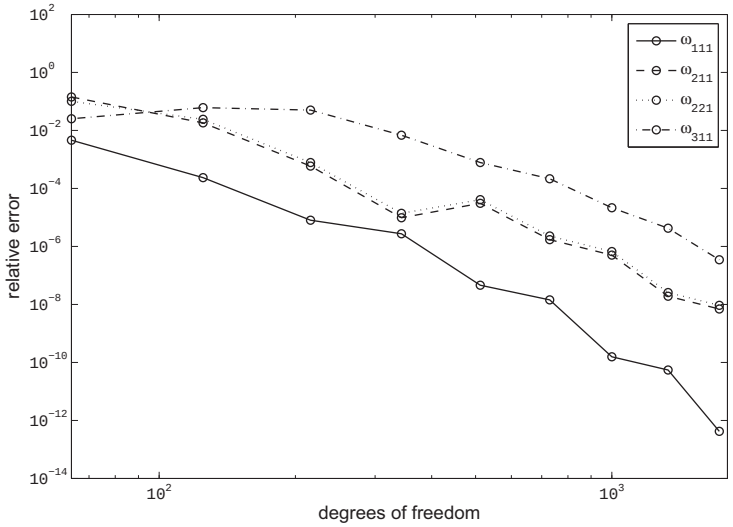

Figure 1: Convergence rate of the first four different Eigenfrequencies.

The third and last simulation deals with the same geometry Ω, but now we want to analyse Robin boundary conditions (see equation (7)). Therefore we take the Eigenfrequency ω_{333} from the second example and compare the related Eigenmmode including reverberative boundary conditions everywhere (see the left part in figure 2) with the related Eigenmode including the Robin boundary condition (see the right part in figure 2) of the form

$$\Omega = \quad [-1,1]^3, \qquad \frac{\partial p}{\partial n}(\vec{x}) + 10p(x) = \quad 0, \quad \forall x \in \partial\Omega. \tag{20}$$

In figure 2 we can see the change of the Eigenmodeshape especially near the boundary, where we alter the reverberative Neumann boundary condition to the Robin boundary condition defined in (20).

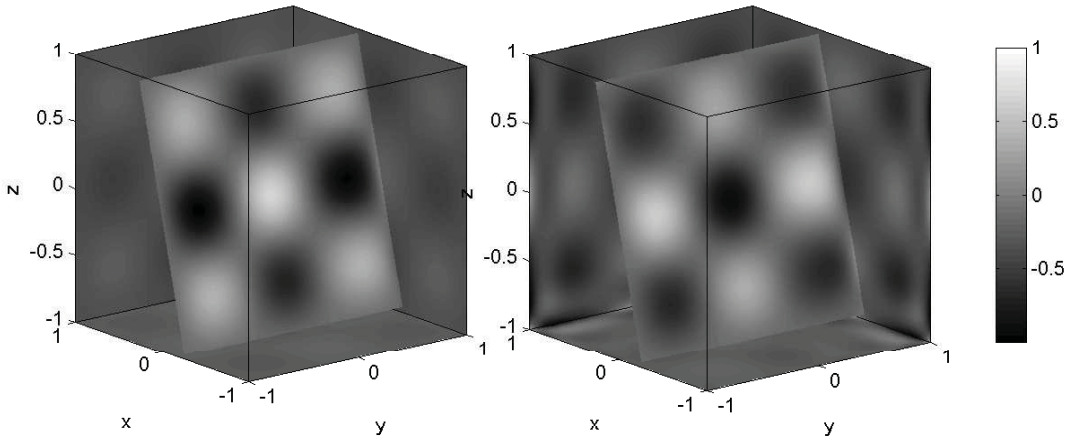

Figure 2: Eigenmodeshape including reverberative (left) and Robin boundary condtions (right)

4 Conclusions and Objectives

In the first chapter we introduced two of the main equations in aeroacoustics, the Wave equation and the Helmholtz equation, as well as the considered combinations of boundary conditions. After that in chapter 2 we derived the theory of the Spectral Method for equispaced and clustered grids. In the following we presented the most important convergence theorems, how to deal with higher dimensions with the help of tensor product grids and the way to include arbitrary boundary conditions. Finally in chapter 3 we applied the method to examples to 3D-benchmark geometries in the time domain as well as in the frequency domain.
The simulation examples verified a very low dispersion and dissipation error without conspicuous spurious oscillations in long-term integrations for the Wave equation, the spectral convergence for analytic solutions and the realisation of arbitrary boundary conditions. Obviously we cannot expand this method to complex geometries. The global approach, in combination with the tensor product grids, only allows simple benchmark geometries like cuboids, spheres and cylinders. Additionally it becomes very fast too expensive to calculate problems with more dimensions and growing degrees of freedom.
Because of these results we want to use the Spectral Method to compare its accurate solutions with solutions of Spectral Finite Element Methods in simple benchmark geometries in the future. The Spectral Finite Element Method should use the advantages of the Spectral Method to simulate complex geometries including realistic boundaries with wave number dependent absorptive characteristics [2].

5 Appendix

In Matlab the discrete Chebyshev Laplacian looks like

$$\begin{aligned}
1D: \quad L_N &= D_N^2 && \in \mathbb{R}^{(N+1)\times(N+1)} \\
2D: \quad L_N &= I_N \otimes D_N^2 + D_N^2 \otimes I_N && \in \mathbb{R}^{(N+1)^2\times(N+1)^2} \\
3D: \quad L_N &= \underbrace{I_N \otimes I_N \otimes D_N^2}_{\approx\frac{\partial^2}{\partial x^2}} + \underbrace{I_N \otimes D_N^2 \otimes I_N}_{\approx\frac{\partial^2}{\partial y^2}} + \underbrace{I_N \otimes I_N \otimes D_N^2}_{\approx\frac{\partial^2}{\partial z^2}} && \in \mathbb{R}^{(N+1)^3\times(N+1)^3} .
\end{aligned} \tag{21}$$

6 Acknowledgement

This research is part of the interdisciplinary project "Room Acoustical Simulations of Realistic Boundary Conditions with Finite Elements" involved in and financed by the International Graduate School of Science and Engineering (IGSSE) of the Technische Universität München (TUM), Project 2.5. We are indebted to Prof. Müller and Martin Buchschmid from the chair of Mechanical Engineering (TUM).

7 References

[1] Arens, K.
Numerische Berechnung thermoakustischer Instabilitäten einer 3D-Benchmark-Brennkammer.
Fortschritt-Berichte VDI, Reihe 20, Nr.403, 2006.

[2] Buchschmid, M., Müller, G.
Modelling of wave number dependent absorptive characteristics with the help of the Theory of Porous Media,
EURODYN (2008)

[3] Canuto, C., M. Hussaini, Y., Quarteroni, A., Zang, T.A.
Spectral Methods: Evolution to Complex Geometries and Applications to Fluid Dynamics.
Springer, Berlin, 2007.

[4] Don, W.S., Solomonoff, A.
Accuracy Enhancement for Higher Derivatives using Chebyshev Collocation and a Mapping Technique.
SIAM Journal on Scientific Computing, vol. 18 , issue 4, pp. 1040 - 1055, 1997.

[5] Schwartzkopff, T., Dumbser, M., Munz, C.-D.
Fast high order ADER schemes for linear hyperbolic equations.
Journal of Computational Physics, vol. 197, pp. 532-539, 2004.

[6] Tam, C.K.W., Webb, J.C.
Dispersion-Relation-Preserving Schemes for Computational Aeroacoustics.
Proceedings of the 14th DGLR/AIAA Aeroacoustics Conference, Aachen, Germany, 1992.

[7] Trefethen, L.N.
Spectral Methods in MATLAB.
Cambridge University Press, 2000.